Supporting Information

Chemical affinity guided high-valence metal oxide interphase engineering for upcycling of ternary cathodes from electric vehicles

Wenyu Wang, [†a] Renming Zhan, [†a] Yuanjian Li, [†b] TianCheng Dong, [a] Zihe Chen, [a] Ruikang Feng, [a] Yida Lu [a] and Yongming Sun*[a]

Formula for calculating the diffusion coefficient in GITT:

$$D = \frac{4}{\pi\tau}\left(\frac{m_B V_M}{M_B S}\right)^2\left(\frac{\Delta E_s}{\Delta E_\tau}\right)^2$$

where D is the Li^+ chemical diffusion coefficient, τ is the pulse duration, m is the mass of active material, M is the molar mass of the active material, V_m is the molar volume of the active material, S is the electrode-electrolyte interfacial area, and ΔE_τ and ΔE_s are the voltage changes during the current pulse and after relaxation to steady state, respectively.

Figure. S1 Photographs of spent 110 Ah LIBs from electric vehicles.

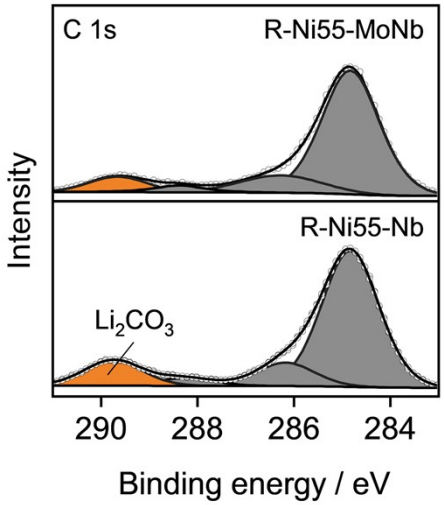

Figure. S2 High-resolution C 1s spectra of R-Ni55-MoNb and R-Ni55-Nb.

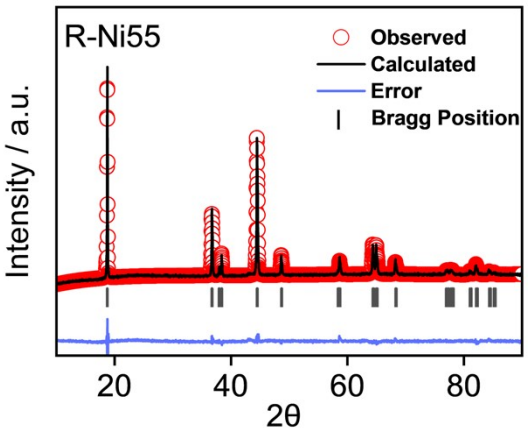

Figure. S3 XRD Rietveld refinement result of R-Ni55.

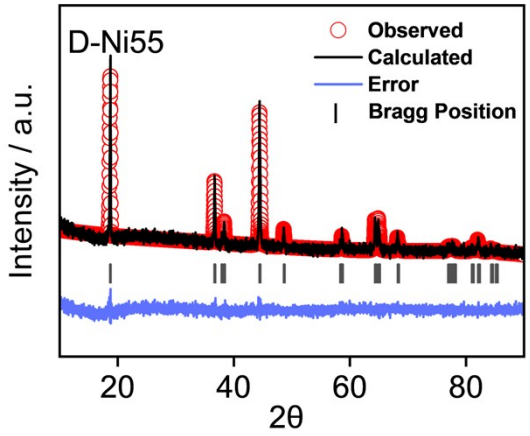

Figure. S4 XRD Rietveld refinement result of D-Ni55.

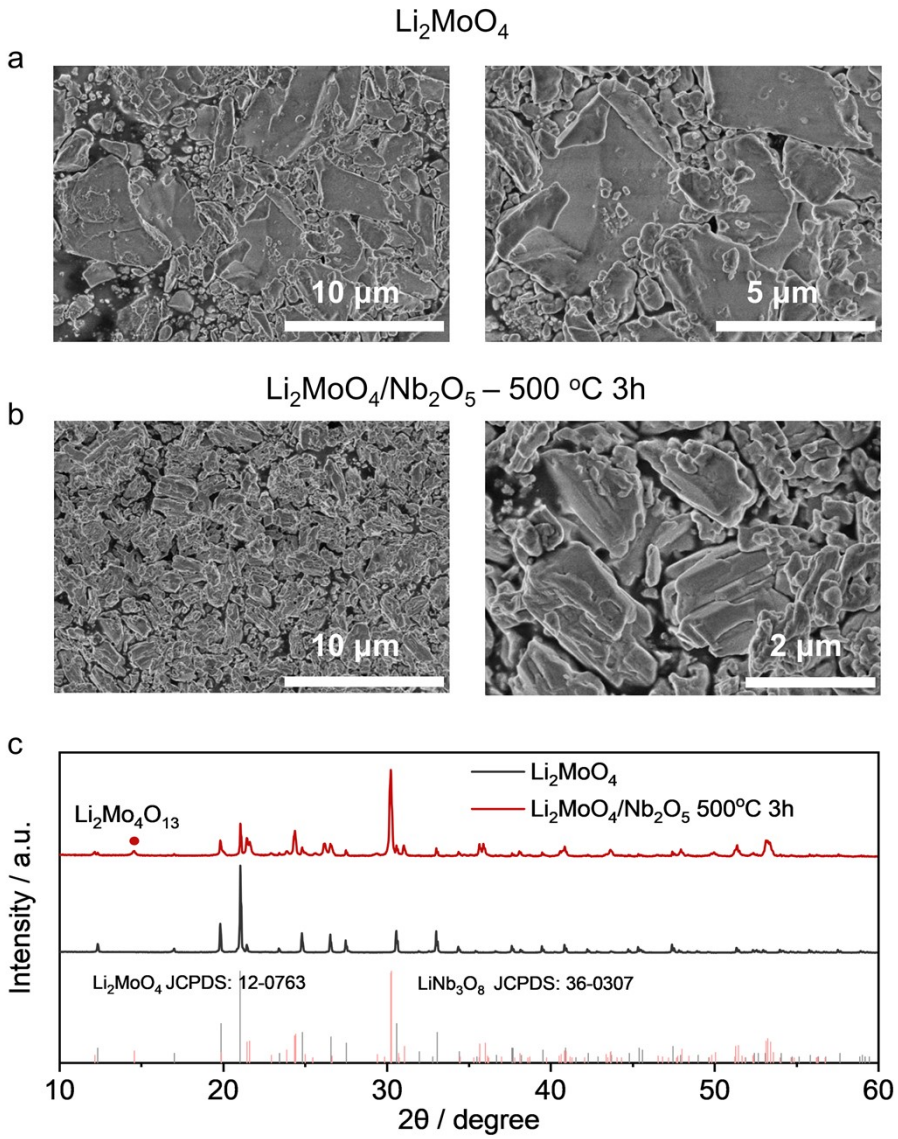

Figure S5. SEM images of (a) pure Li_2MoO_4 and (b) the reaction product of Li_2MoO_4/Nb_2O_5 (1:1 molar ratio) after annealing at 500 °C for 3 h. (c) XRD patterns of Li_2MoO_4 and the reaction product of Li_2MoO_4/Nb_2O_5 (1:1 molar ratio) after annealing at 500 °C for 3 h.

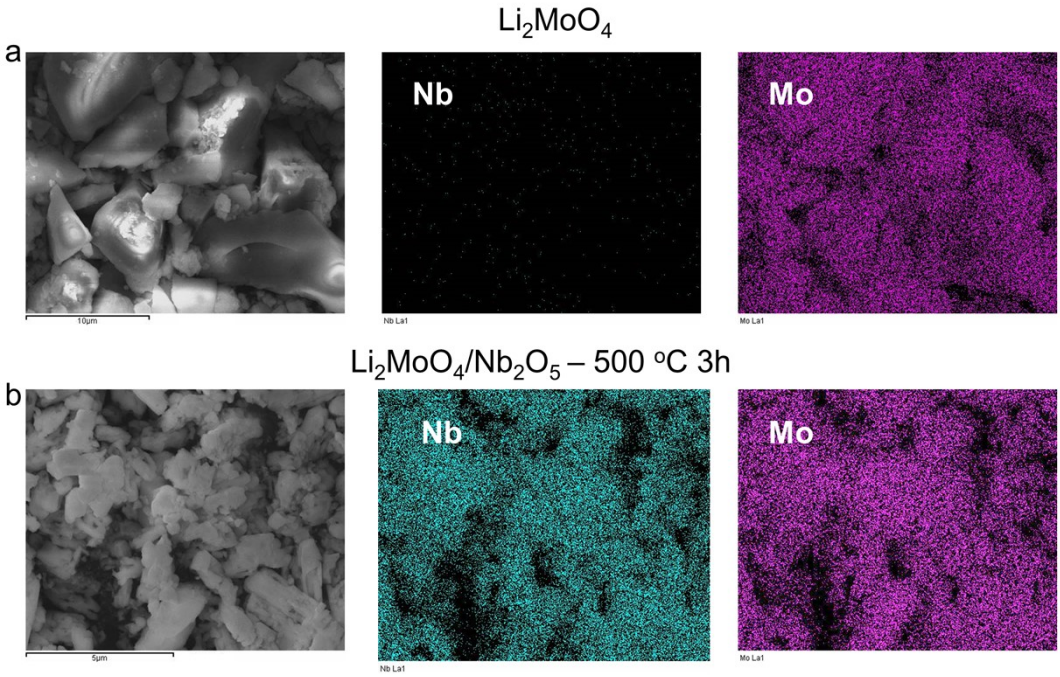

Figure S6. SEM-EDS results of (a) pure Li_2MoO_4 and (b) the reaction product of Li_2MoO_4/Nb_2O_5 (1:1 molar ratio) after annealing at 500 °C for 3 h.

To further examine the interaction between Mo- and Nb-containing species, pure Li_2MoO_4 was synthesized, as shown in Figures S6a. Li_2MoO_4 was then mixed with Nb_2O_5 at a 1:1 molar ratio and heated at 500 °C for 3 h. The reaction product exhibited pronounced morphological changes and additional diffraction peaks (Figures S6b and c), indicating the formation of a new phase. During this process, Li_2MoO_4 serves as a lithium source and reacts with Nb-containing species to form $LiNb_3O_8$. Energy-dispersive X-ray spectroscopy (EDS) mapping (Figure S6) revealed that Mo and Nb were homogeneously distributed in the product, evidencing strong chemical interactions between Li_2MoO_4 and Nb_2O_5 during the thermal reaction.

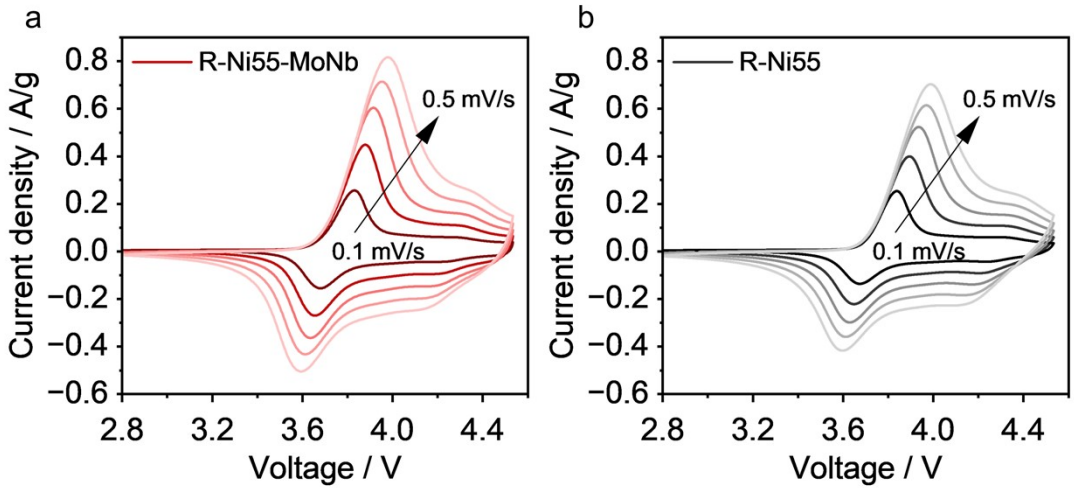

Figure S7. CV curves of (a) R-Ni55-MoNb and (b) R-Ni55 at different scanning rates (0.1-0.5 mV/s).

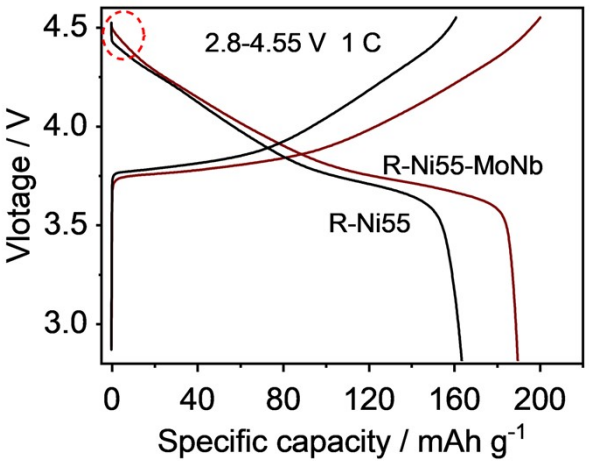

Figure S8. Charge-discharge profiles of R-Ni55 and R-Ni55-MoNb for the 1st cycles at 1 C.

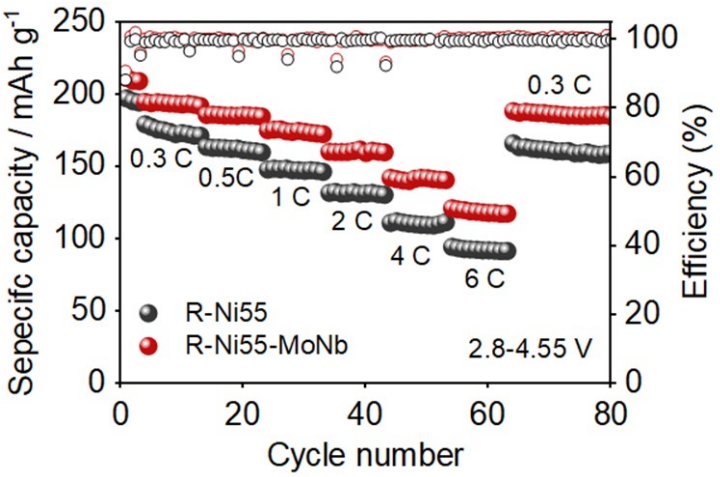

Figure S9. Rate performance of R-Ni55 and R-Ni55-MoNb.

The rate performances are compared in Figure S9. R-Ni55-MoNb delivered discharge capacities of 212, 195, 186, 175, 161, 142, and 121 mAh g^{-1} at 0.1, 0.3, 0.5, 1, 2, 4, and 6 C, respectively, while R-Ni55 exhibited 197, 180, 164, 148, 132, 111, and 95 mAh g^{-1} at the same rates. Upon returning to 0.3 C, the capacity retention was 96% for R-Ni55-MoNb and 92% for R-Ni55.

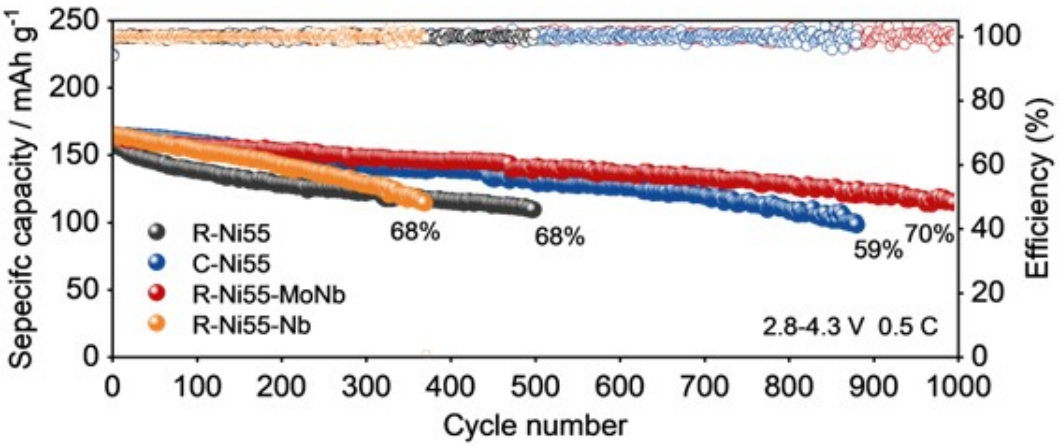

Figure S10. Cycling performance of R-Ni55, C-Ni55, R-Ni55-Nb and R-Ni55-MoNb half cells at 0.5 C within 2.8-4.3 V.

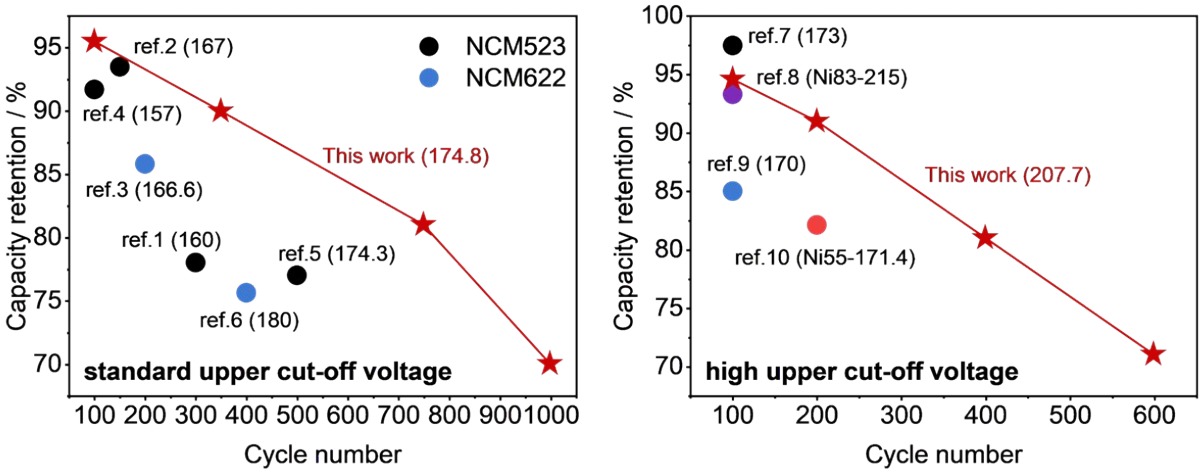

Figure S11. Cycling performance and reversible capacity of R-Ni55-MoNb compared with regenerated NCM cathodes reported in recent studies (corresponding to Table S6).

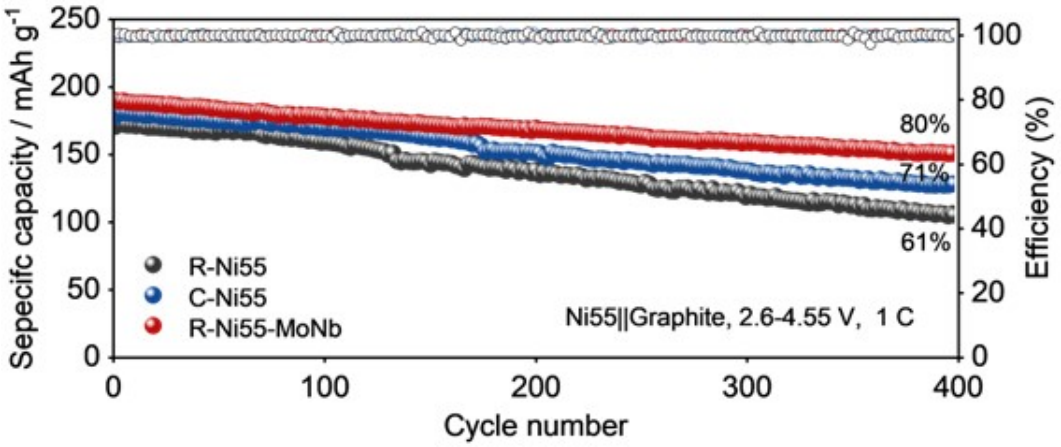

Figure S12. Cycling performance of R-Ni55, C-Ni55, and R-Ni55-MoNb full cells at 1 C within 2.6-4.55 V.

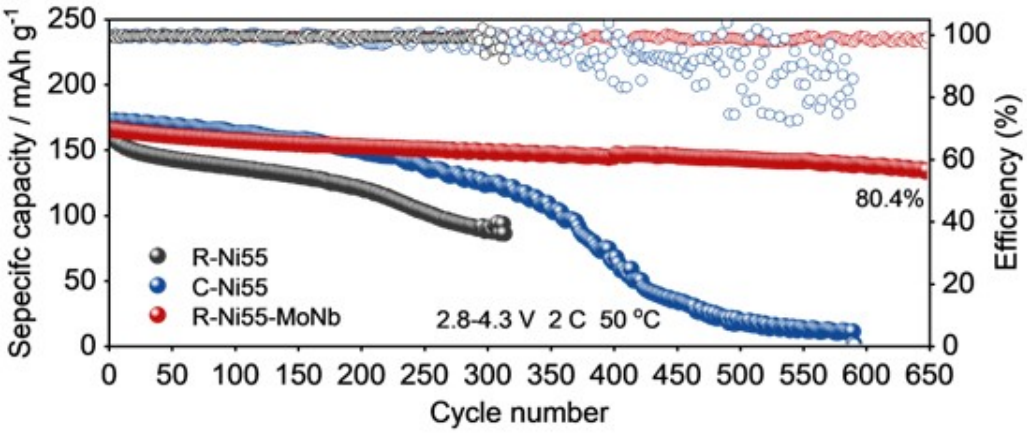

Figure S13. Cycling performance of R-Ni55, C-Ni55, and R-Ni55-MoNb half cells at 2 C within 2.8-4.3 V (50 °C).

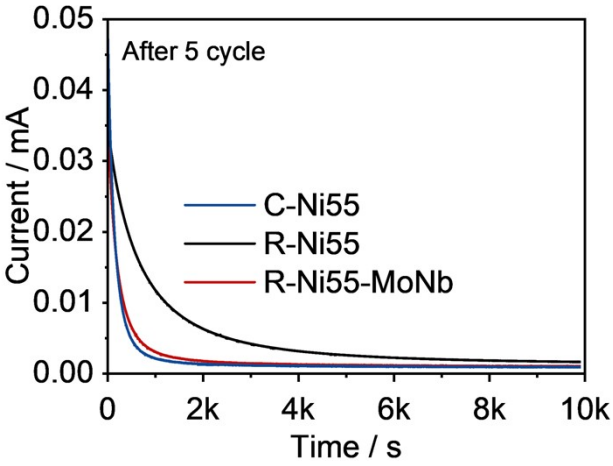

Figure S14. Leakage current profiles of R-Ni55, C-Ni55, and R-Ni55-MoNb half cells after 5 cycles.

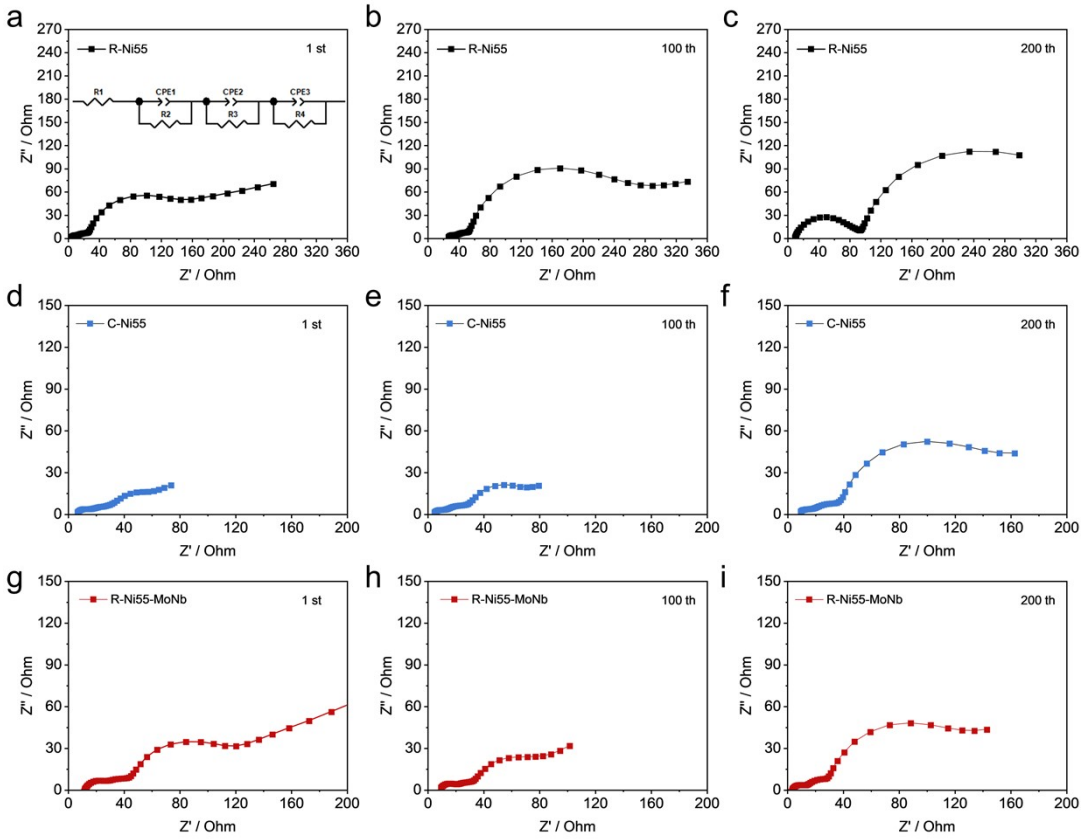

Figure S15. Nyquist plots of (a-c) R-Ni55, (d-f) C-Ni55, and (g-i) R-Ni55-MoNb after 1, 100, and 200 cycles, respectively, recorded in the frequency range 100 kHz-100 mHz.

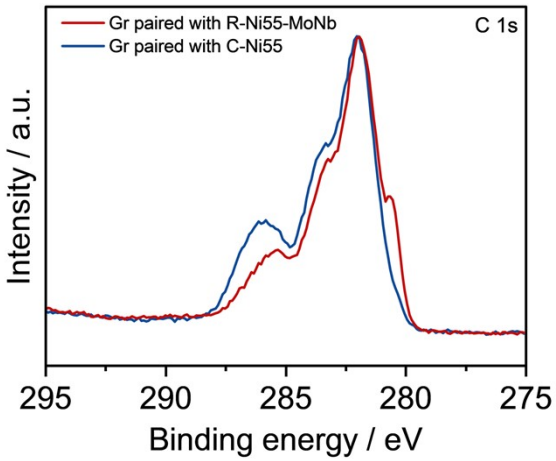

Figure S16. High-resolution XPS spectra of C 1s for graphite electrode paired with C-Ni55 and R-Ni55-MoNb electrodes.

Table S1. Energy consumption of different recycling approaches (MJ kg^{-1} cell)

	Material Input	Energy Input	Total
Pyro	6.364	5.985	12.349
Hydro	17.510	2.060	19.570
General-direct	11.663	9.254	20.917
This work	3.983	4.979	8.963

The energy consumption of four recycling/regeneration routes was evaluated for comparison, including our solid-state upcycling process (this work), a general direct-regeneration route for NCM cathodes (General-direct), pyrometallurgical recycling (Pyro), and hydrometallurgical recycling (Hydro). The life-cycle energy demand was estimated using the EverBatt model developed by Argonne National Laboratory, assuming an annual plant processing capacity of 10,000 tons of spent Ni55 cells.

Table S2. Molar ratio of Li, Ni, Co, Mn elements in different Ni55 samples according to the Inductively Coupled Plasma Optical Emission spectroscopy (ICP-OES) results.

	Measure atomic ratio			
Sample	Li	Ni	Co	Mn
D-Ni55	0.8760	0.5571	0.1498	0.2932
R-Ni55	1.0314	0.5515	0.1515	0.2971
R-Ni55-MoNb	1.0776	0.5653	0.1474	0.2873
C-Ni55	1.0172	0.5572	0.1501	0.2927

Table S3. Structural parameters obtained from Rietveld refinement of XRD pattern of R-Ni55-MoNb. (a=b= 2.87086 Å c = 14.23500 Å Unit-cell volume = 101.604Å^3, Rp=2.01%, Rwp=2.63%)

atom	site	Wyckoff positions			occupancy
Li1	3b	0	0	0.5	0.984
Li2	3a	0	0	0	0.016
Ni1	3b	0	0	0.5	0.016
Ni2	3a	0	0	0	0.527
Mn	3a	0	0	0	0.305
Co	3a	0	0	0	0.152
O	6c	0	0	0.25935	1.000

Table S4 Structural parameters obtained from Rietveld refinement of XRD pattern of R-Ni55.(a=b= 2.86897 Å c = 14.22650 Å Unit-cell volume = 101.410 Å^3, Rp=3.49%, Rwp=2.51%)

atom	site	Wyckoff positions			occupancy
Li1	3b	0	0	0.5	0.943
Li2	3a	0	0	0	0.057
Ni1	3b	0	0	0.5	0.057
Ni2	3a	0	0	0	0.486
Mn	3a	0	0	0	0.305
Co	3a	0	0	0	0.152
O	6c	0	0	0.25340	1.000

Table S5. Structural parameters obtained from Rietveld refinement of XRD pattern of D-Ni55. (a=b= 2.87190 Å c = 14.23700 Å Unit-cell volume = 103.166 Å^3, Rp=4.63%, Rwp=5.85%)

atom	site	Wyckoff positions			occupancy
Li1	3b	0	0	0.5	0.808
Li2	3a	0	0	0	0.072
Ni1	3b	0	0	0.5	0.072
Ni2	3a	0	0	0	0.469
Mn	3a	0	0	0	0.310
Co	3a	0	0	0	0.150
O	6c	0	0	0.25450	1.000

Table S6. Summary of related reports on performance of the direct regenerated NCM.

Electrode	Voltage window	Specific capacity (mAh g^{-1})	Capacity retention (%)	Ref.
Ni55	**2.8-4.3 V**	**174.8 at 0.1 C 163.3 at 0.5 C**	**350 cycles 90% at 0.5 C 750 cycles 81% 1000 cycles 70%**	**This work**
NCM523	2.8-4.3 V	160 at 0.5 C	300 cycles 78% at 0.5 C	1
NCM523	2.8-4.3 V	167.0 at 0.1 C 152.5 at 1 C	150 cycles 93.5% at 1 C	2
NCM622	2.8-4.3 V	166.6 at 0.1 C 153.3 at 1 C	200 cycles 85.8% at 1 C	3
NCM523	2.8-4.3 V	157.0 at 0.1 C 139.6 at 1 C	100 cycles 91.7% at 1 C	4
NCM523	3.0-4.3 V	174.3 at 0.1 C	500 cycles 77% at 0.5 C	5
NCM622	2.5-4.3 V	180 at 0.1 C 160 at 0.5 C	400 cycles 75.6% at 0.5 C	6
Ni55	**2.8-4.55 V**	**207.7 at 0.1 C 182.9 at 1 C**	**200 cycles 91% at 1 C 400 cycles 81% 600 cycles 71%**	**This work**
NCM523	3.0-4.5 V	173 at 0.2 C	100 cycles 97.5% at 0.2 C/1 C	7
NCM83	2.6-4.6 V	215 at 0.1 C	100 cycles 93.3% at 1 C	8
NCM622	3.0-4.6 V	170 at 0.1 C	100 cycles 85% at 1 C	9
Ni55	2.8-4.4 V	171.4 at 0.1 C	200 cycles 82.1% at 0.3 C	10

Table S7. Fitting results of ohmic impedance (R1), CEI impedance (R2), SEI impedance (R3), and charge transfer impedance (R4) of the cycled Ni55.

		R1	R2	R3	R4
1st	R-Ni55	3.4	8.1	13.9	144.0
	C-Ni55	5.8	8.6	15.3	53.3
	R-Ni55-MoNb	11.8	16.7	14.0	96.5
100th	R-Ni55	25.6	13.6	11.7	240.4
	C-Ni55	3.7	7.9	18.2	54.9
	R-Ni55-MoNb	8.4	12.8	9.4	73.9
300th	R-Ni55	9		80.9	321.3
	C-Ni55	7.2	11.5	18	135.5
	R-Ni55-MoNb	3.4	9.6	15.9	120.9

Reference

1 Z. Zhuang, J. Li, H. Ji, Z. Piao, X. Wu, G. Ji, S. Liu, J. Ma, D. Tang, N. Zheng, J. Wang, G. Zhou. *Adv. Mater.* **2024**, 36, 2313144.

2 M. Fan, X.-H. Meng, H. Guo, S. Xin, X. Chang, K.-C. Jiang, J.-C. Chen, Q. Meng, Y.-G. Guo. *Adv. Mater.* **2024**, 36 (35), 2405238.

3 Y. Liu, H. Zhang, J. Wang, X. Chen, Q. Li, Y. Zhou, K. Sun, X. Zhao. *Chem. Eng. J.* **2025**, 514, 162855.

4 Z. Xiao, Y. Yang, Y. Li, X. He, J. Shen, L. Ye, F. Yu, B. Zhang, X. Ou. *Small.* **2024**, 20 (26), 2309685.

5 S. Jin, Z.-A. Lu, D. Mu, T. Lin, W. Zhang, Y. Zhang, D. Chen, R. Li, C. Dai. *Adv. Funct. Mater.* **2024**, 2416085.

6 Wang, J.; Ji, H.; Li, J.; Liang, Z.; Chen, W.; Zhu, Y.; Ji, G.; Shi, R.; Zhou, G.; Cheng, H.-M. *Nat. Sustain.* **2024**, 7 (10), 1283-1293.

7 H. Dong, H. Wang, J. Qi. J. Wang, W. Ji, J. Pan, X. Li, Y. Yin, S. Yang. *ACS Sustain. Chem. Eng.* **2022**, **10**, 11587-11596.

8 H. Ji, J. Wang, H. Qu, J. Li, W. Ji, X. Qiu, Y. Zhu, H. Ren, R. Shi, G. Ji, W. Zhao, G. Zhou. *Adv. Mater.* **2024**, 36, 2407029.

9 C. Zhu, H. Zhao, T. Xu, W. Tang, Y. Zhang, L. Li, Y. Li, X. Wang, M. Sun, Z. Sun. *J. Mater. Chem. A.* **2025**, 13, 25093-25102.

10 Y. Guo, Y. Li, K. Qiu, Y. Li, W. Yuan, C. Li, X. Rui, L. Shi, Y. Hou, S. Liu, D. Ren, T. Tan, G. Zhu, L. Lu, S. Xu, B. Deng, X. Liu, M. Ouyang. *Energy Environ. Sci.* **2025**, 18 (1), 264-274.